Aerothermal Characteristics of Transonic Over-Tip Leakage Flow for Different Tip Geometries with Cooling Injection

Mingxing Tang

Master Candidate, School of Aeronautics and Astronautics,

Shanghai Jiao Tong University,

Shanghai 200240, China

E-mail: Startown@sjtu.edu.cn

Shaopeng Lu[1]

Research Associate, School of Aeronautics and Astronautics,

Shanghai Jiao Tong University,

Shanghai 200240, China

E-mail: lusp@sjtu.edu.cn

Yunkai Liu

Master Candidate, School of Aeronautics and Astronautics,

Shanghai Jiao Tong University,

Shanghai 200240, China

E-mail: sjtu10018lyk@sjtu.edu.cn

Jinfang Teng

Professor, School of Aeronautics and Astronautics,

Shanghai Jiao Tong University,

Shanghai 200240, China

E-mail: tjf@sjtu.edu.cn

Abstract: In turbomachinery, the effect of cooing injection on the over-tip leakage (OTL) flow has been the focus. In the present work, the flow and heat transfer on the blade tip surfaces of two typical different tip structures including a flat tip and a squealer tip are investigated. The grid independence verification and turbulence model validation (including Shear Stress Transport k-ω model and Spalart-Allmaras model) are conducted. And some numerical results are compared with the existing experimental results. It is found that the shock wave structures produce near the pressure side corner and a high striped pressure coefficient region appears on the tip surface near the pressure side. The cooling injection could alter the range of high striped pressure coefficient region. The tip leakage vortex (TLV) was formed by the blending between the OTL flow and mainstream, causing a large aerodynamic penalty. In comparison, the flat tip shows a greater loss near the casing and the tip surface than the squealer tip. An interesting observation is that the coolant ejecting from the cooling jet hole bifurcates and then forms a counter-rotating vortex pair (CRVP) for both the flat tip and the squealer tip, which greatly changes the flow structures and heat transfer characteristics within the tip region. The branches of the CRVP cause the thermal stripes on the surfaces of blade tip and the suction side rim. The present results reveal

the cooling injection has a strong effect on OTL flow and enlighten the design and optimization of blade tips.

Keywords: aerodynamic, heat transfer, over-tip leakage flow, cooling injection, tip geometries

1 Corresponding Author

1 Introduction

In modern gas turbines, a continuous increase in turbine inlet temperature has improved the turbine thermal efficiency. Meanwhile, the large thermal load caused by such high temperature makes the turbine tips one of the most susceptible parts. There exists a clearance between turbine blade tip and the casing, and the gas driven by the pressure difference crosses the tip surface and forms the over-tip leakage flow. The resulting leakage flow loss is an important part of the stage losses in high pressure turbine (HPT). As a result, comprehensive research on heat transfer and aerodynamics over the blade tip regions has been more and more significant for investigators nowadays.

Many numerical simulations have been carried out to study the aero-thermal characteristics. The effects of tip clearance heights and casing recess on stage efficiency and heat exchange for different squealer tip geometries were investigated by Ameri et al. [1]. It was found that the heat transfer on the pressure side (PS) was decreased when the recessed casing was introduced. A marked reduction of thermal load could be observed on the blade tip regions. Ameri and Bunker [2] conducted a numerical study of the heat transfer performances on turbine blade tip surfaces for a large-power generation turbine and the computational results were compared with the experimental results reported by Bunker [3]. Ameri [4] compared the results of a mean-camber line strip tip with a sharp edge tip, and it was found that a sharp edge tip works better in reducing the tip leakage loss and the tip heat transfer. Considering three different tip geometries of baseline flat tip, cavity tip and suction side (SS) squealer tip, Krishnababu et al. [5] numerically studied the effects of diverse tip geometries on aero-thermal characteristics in unshrouded axial flow turbines. Their results revealed that the leakage mass flow and the heat transfer on tip regions increased as the tip gap heights increased. Krishnababu and Newton et. al. [6,7] also examined the effects of relative casing motion and coolant injection on the aerodynamics and heat exchange of the OTL flow. Yang et al. [8,9] performed the similar studies as well. Their conclusions showed that although the heat transfer coefficient (HTC) decreased as the cavity depth increased., the shallow cavity is the more effective configuration to decrease the large thermal load. Also, the GE-E3 blade with two different tip geometries, flat tip and squealer tip, were used by Yang et al. [10,11] to study the flow and heat transfer, and distributions of HTC were in satisfactory agreement with the experimental results reported by Azad et al. [12,13].

Lots of experiments have been performed to investigate the aerodynamic and heat transfer characteristics on the blade tip areas. With the transient liquid technique, a two-dimensional model of first stage gas turbine rotor blade was studied by Azad et al. [12,13]. The detailed static pressure distributions and HTC on flat and squealer tip surfaces were measured, and the effects of the tip gap size are considered as well. Using the same research technique and blade models, Kwak and Han [14,15] discussed the effects of blowing ratio and tip gap sizes as the coolant injection was introduced. Their results showed that the overall film-cooling effectiveness increased with increasing blowing, and the overall heat exchange enhanced with increasing tip gap size. Kwak et al. [16] further studied the effects of the positions of squealer rims, and it was found that the suction side squealer tip provided the lowest HTC on the blade tip and near tip regions compared to the other layouts. In order to assess the overall film-cooling benefit of the pressure side blowing, Christophel et al. [17,18] measured the adiabatic effectiveness levels and the HTC.

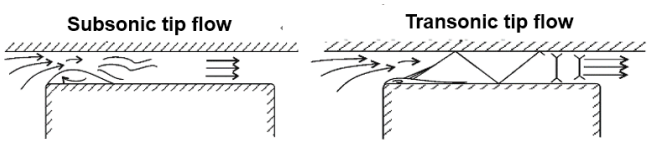

Fig. 1 Schematics of subsonic and transonic tip flow structure [19]

The typical characteristics of a subsonic tip flow and a transonic tip flow were shown in Figure 1. Zhang et al. [20] reported that the shock wave structure in transonic OTL flow greatly influenced the heat transfer on tip surface. The contours of the multiple reflected shock wave structure were clearly visible. Some researchers such as Couch et al. [21] and Wheeler et al. [22,23] investigated the effects of tip coolant injection on transonic OTL loss. Similarly, Ma et al. [24,25] numerically and experimentally studied the transonic squealer tip with the cooling injection. It was observed that dominant driving flow structure was a counter-rotating vortex pair (CRVP) caused by the bifurcation of coolant impinging on the casing. Such CRVP was responsible for the emergence of high thermal stripes on the tip regions.

The present numerical study focuses on the flow and heat transfer on the blade tip regions with two different tip geometries including a flat tip and a squealer tip. The strong interactions between OTL flow and cooling injection has

been discussed. A part of the computational results was compared with the experimental results of Ma et al. [24,25].

2 Numerical methods

The commercially available CFD solver, ANSYS-CFX, was employed in present numerical calculations. By solving the steady Reynolds-averaged Navier-Stokes (RANS) equations, the computational results are obtained. Two different turbulence models, the Spalart-Allmaras (SA) model and the Shear Stress Transport k-ω model (SST k-ω), are selected to verify the grid dependence and compare the experimental results. All high-quality structured meshes are generated by using ICEM software.

2.1 Computational Model and Mesh

The blade model with cooling jet holes is presented in Figure 2(a), This model shares the same blade profile in Ma [1], but the cooling jet holes differs. The tip clearance height and the cooling hole diameter share the same size of 0.675mm. Five cooling holes are located along the camber lines and the distance between two adjacent holes equals 5 times of the hole diameter. As is shown in Figure 2(b), four diverse tip geometries, including cooled/uncooled flat and cooled/uncooled squealer tips, are chosen to implement current research.

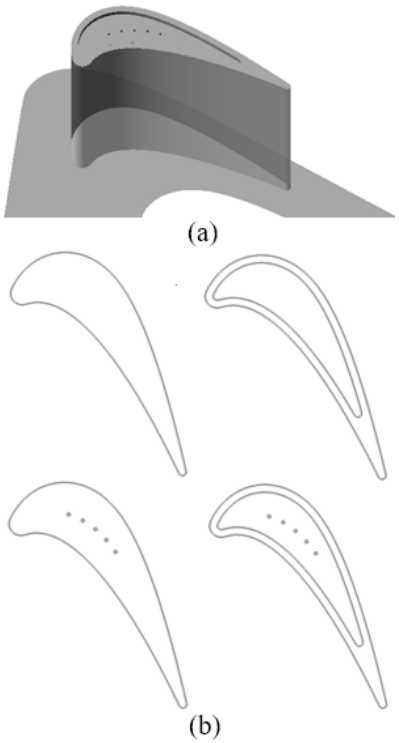

Fig. 2 Geometric model and four different blade tips

As shown in Figure 3, the computational domain is a single-channel fluid domain with translational periodic boundaries and the structured mesh is clearly visible.

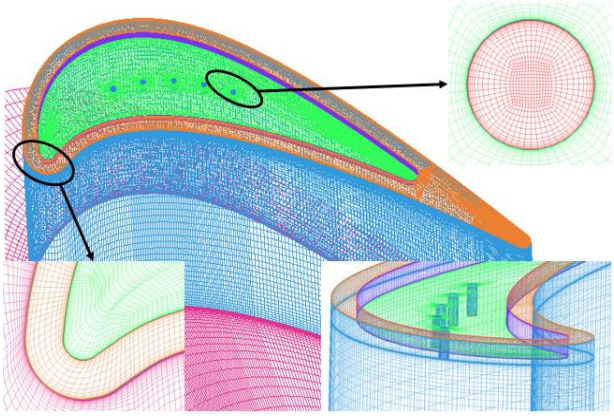

Fig. 3 Computational domain and meshes

The total pressure and total temperature boundary conditions are specified to the inlet and cooling holes, and the outlet is set to be the static pressure boundary. The hub is specified as a symmetric boundary. All walls are set as the no-slip isothermal boundary conditions. Some specific boundary conditions are listed in Table 1.

Table 1 Part of boundary conditions

Inlet total pressure $P_{0,in}$ (kPa)	180
Inlet total temperature $T_{0,in}$ (K)	300
Inlet flow angle (°)	45.3
Coolant total pressure $P_{0,c}$ (kPa)	198
Coolant total temperature $T_{0,c}$ (K)	150
Outlet static pressure P_{exit} (kPa)	101
Wall temperature T_w (K)	280/290

2.2 Grid Independence Study

Table 2 lists the detailed characteristics of the computational grids used in grid independence study. Increasing the grid nodes within the tip clearance and cavity heights, the total grid elements, as shown in Table 2, have changed from 3.65×10^6 to 5.74×10^6. The average y+ value over the tip regions is around 0.8 for all cases.

Table 2 Grid details of 3D computational domains

Grid Number(million)		3.65	4.70	5.74	6.97
Grid Points within Tip Gap	SA/SST	20	30	40	50
Grid Points within Cavity Height	SA/SST	30	40	50	60
Average y+ on Tip Surfaces	SA	0.7687	0.7782	0.8190	0.8273
	SST	0.8096	0.8070	0.8047	0.8039
Average HTC (W/m2·K)	SA	1156.8	1125.3	1113.2	1110.9
	SST	1135.7	1148.9	1154.0	1157.4

Figure 4 shows the relative HTC difference between different grid sizes. In comparison, the local HTC difference between 5.74×10^6 and 6.79×10^6 elements is less than 1.5% for the most of the tip surface. Besides, when the number of grid elements increases from 3.65×10^6 to 5.74×10^6, the change of average HTC on the tip surface is relatively large. However, such a change becomes pretty

slight as the total grid elements further grow into 6.97×10^6. In other words, the influence of introducing more grid elements will be negligible. Consequently, the number of 5.74×10^6 elements is selected for the present research.

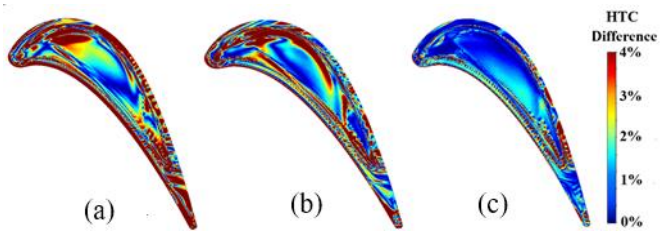

Fig. 4 Relative HTC difference among the different grid quantities (a) 3.65 and 4.70 million (b) 4.70 and 5.74 million (c) 5.74 and 6.97 million

2.3 Turbulence Model Validation

Based on the experimental results (Ma et al. [25]), the HTC distributions of numerical simulations with SST *k*-*ω* model and SA model are shown in Figure 5. By contrast, the difference in the distribution of HTC on the blade tip surface is pretty evident.

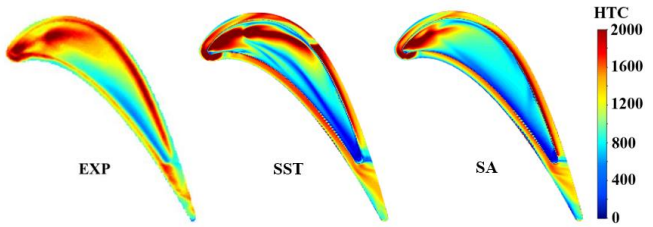

Fig. 5 Comparison of HTC on the tip surfaces between numerical results (SST *k*-*ω* model and SA model) and experimental results

As shown in Figure 5, the overall HTC distributions for SST *k*-*ω* model and SA model are in good agreement with the experimental results, especially for the low HTC regions on the cavity floor close to the pressure side and the high HTC regions near the leading edge. Comparing the range of high HTC regions on the cavity floor and the rim surfaces, it is obvious that the SST *k*-*ω* model shows a better prediction on the high HTC regions than the SA model. Similar results were reported by Ma et al. [32,33]. It means the SST *k*-*ω* model is more suitable and accurate than SA model in simulating the near wall flow in the present study.

3 Results and Discussions

3.1 Effects of Shock Wave Structure and Pressure Coefficient

The nondimensional pressure coefficient C_p is employed to describe the distributions of the relative pressure. The definition of C_p is

$$C_p = \frac{P_{0,in} - P}{P_{0,in} - P_{exit}} \quad (1)$$

where the $P_{0,in}$ is the total pressure of the inlet fluid, P is the local static pressure, and the P_{exit} is the static pressure of the fluids at the exit.

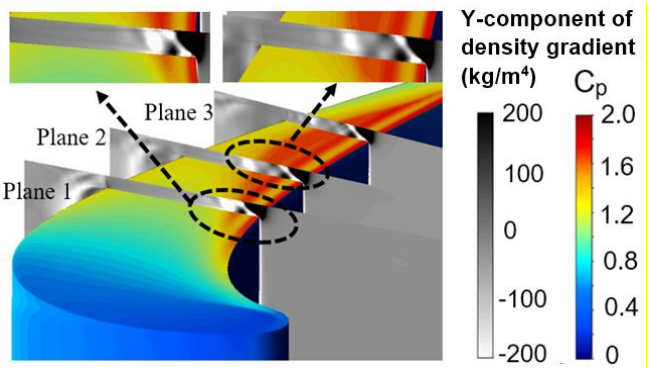

Fig. 6 Contours of Y-component of density gradient (kg/m4) distributions on three cut-planes and the pressure coefficient over the flat tip

To better elaborate the aerodynamic performance within the tip gap, the contours of Y-component of density gradient distributions on three cut-planes and C_p on the uncooled flat tip are presented in Figure 6. The shock waves within the tip gap are evidently visible on those cut-planes. The reflected shock wave (the oblique shock wave) appears near the pressure side edge. And a normal shock wave is generated along the border of the high striped C_p region. Note that the range of shock wave in plane 1 is smaller than that in plane 2. This is because most of the area of plane 1, namely, the downstream of the high striped C_p border, is in subsonic state. It is observed that the pressure load increases when the shock waves hitting the tip surface. Similar conclusions were reported by Zhang et al. [20].

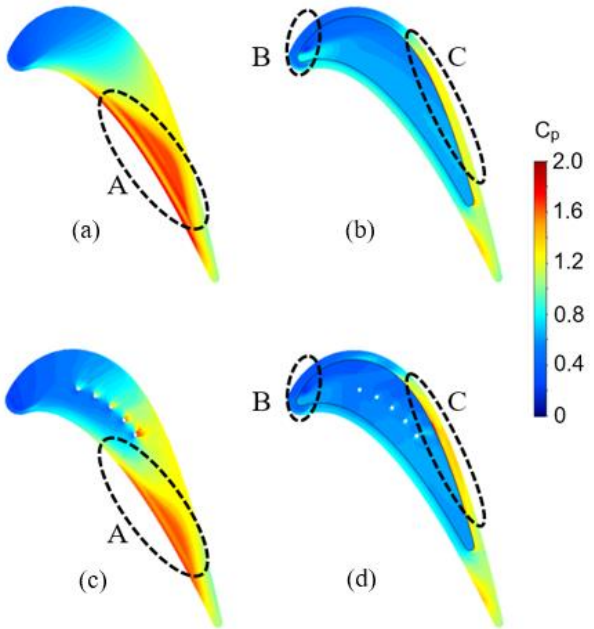

Fig. 7 Distributions of pressure coefficient on different blade tip surfaces: (a) uncooled flat and squealer tips (b) cooled flat and squealer tips

The results of pressure coefficients on the tip surfaces of four different tip geometries are plotted in Figure 7. The averaged pressure coefficient of flat tip surfaces, both for uncooled and cooled cases, is higher than that of squealer tip surfaces. In other words, the introduction of groove for squealer tips decreases the pressure load over the blade tip surfaces. The frontal parts for given cases stand a low C_p region, and the minimum C_p for squealer tips occurs inside the region B. It means a less pressure difference to drive the fluid across the tip gap. it is seen that the C_p shows a striped distribution in region A, and its border is consistent with the profile of low HTC stripe (marked B) in Figure 12(a). The flow in this region is transonic and the reflected shock wave captured through density gradient is shown in Figure 6. Compared with the uncooled flat tip, the size of the high C_p region for cooled flat tip shrinks with the introduction of cooling holes. The values of C_p in region C of suction side, for the uncooled and cooled squealer tips, are bigger than those on the rim surfaces of the pressure side. The reason for such a difference is that flow separation zone on the rim surface of suction side is larger than that on the rim surface in the pressure side.

3.2 Effect of Cooling Injection on Transonic OTL Flow

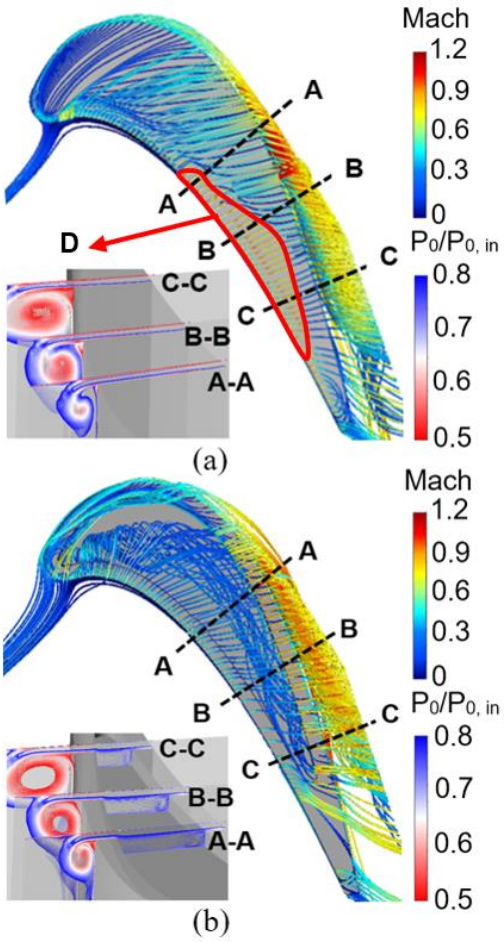

Fig. 8 Stagnation pressure ratio ($P_0/P_{0,in}$) along three cut-planes and the OTL flow streamlines over the tip surfaces

Figure 8 shows the OTL flow patterns over the flat and squealer tip surfaces, and the stagnation pressure ratio contours on three cut-planes are presented as well. For the flat tip in Figure 8(a), the flow separates as it enters the tip gap and then reattaches. Driven by the big pressure difference, the OTL flow goes to the suction side and blends with the mainstream, forming the tip leakage vortex (TLV). It is observed that the considerable aerodynamic penalty was caused by such TLV. The local stagnation pressure ratio in TLV core region is even below 50%. The Mach number in region D is relatively higher than other parts of the flat tip and the flow is in transonic condition. This region is consistent with the high C_p region where the shock waves occurred.

For the squealer tip in Figure 8(b), the flow separation still exists at the entrance of the pressure side, but no flow attachment happens on the surface of the pressure side rim. A part of the flow goes into the groove and then forms the vortices. The Mach number of these flow is small. Note that the similar TLV and the resulting aerodynamic penalty could be observed for the squealer tip as well. However, the flat tip apparently shows a smaller stagnation pressure ratio near the casing and the tip surface than the squealer tip.

Figure 9 shows the nondimensional averaged mass flux distributions of the OTL flow along the suction side edge. Compared to the flat tip, it is evident that the squealer tip reduces the OTL mass flux, especially in the frontal part. When the cooling injection is introduced, a slight increase of OTL mass flux is observed in the frontal part. Then, a zigzag line could be vividly found in the mid-chord (x/C_x = 30-60%) region. This is mainly due to the discrete layout of the cooling holes. From the region of x/C_x > 60%, there is no big difference of OTL mass flux for all cases. However, a considerable reduction of OTL mass flux exists near the region of x/C_x = 80%.

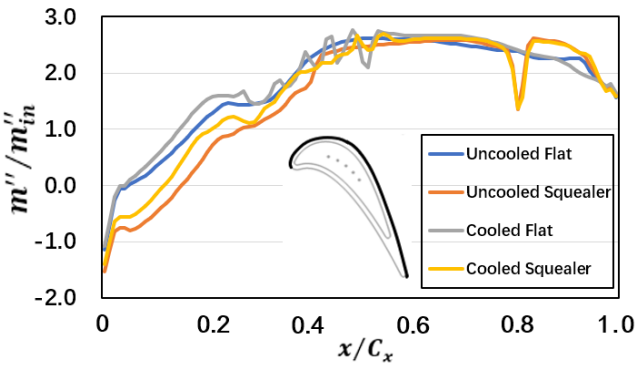

Fig. 9 Nondimensional averaged OTL mass flux distribution along the suction side edge

Figure 10 shows the flow structure of the cooling injection for the cooled squealer tip. Driven by the upstream OTL flow and the casing, the coolant bifurcates in Figure 10(a) and Figure 10(c), and the counter-rotating vortex pair (CRVP) is formed since these two branches rotate in opposite directions. Starting from the leading edge, it is observed that the diffusion range of coolant ejecting from cooling holes is getting smaller around every cooling hole, while the local Mach number is becoming bigger and bigger.

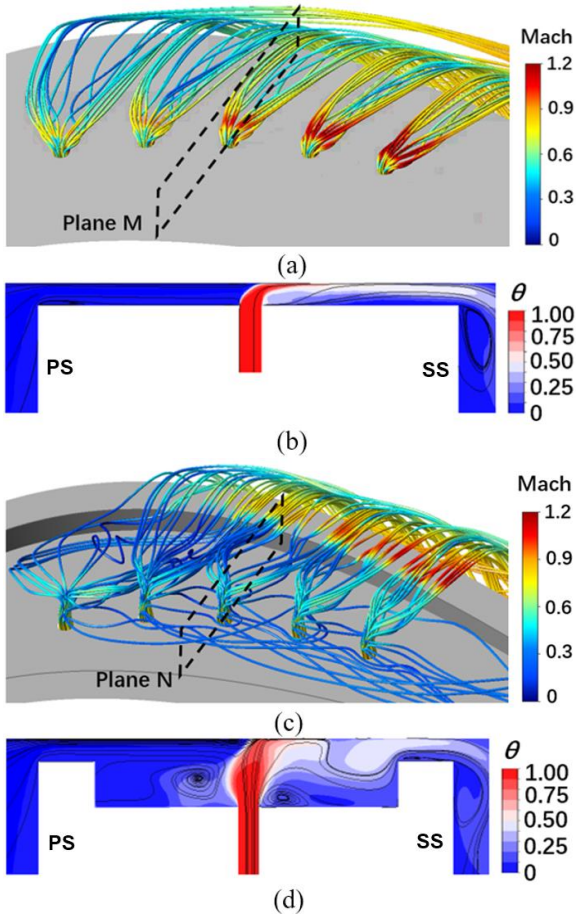

Fig. 10 Flow structure of cooling injection

To better explore the interaction between coolant and OTL flow, the nondimensional total temperature θ is defined to describe such interaction in Figure 10(b) and Figure 10(d). The expression of θ is

$$\theta = \frac{T_{0,in} - T_0}{T_{0,in} - T_c} \tag{2}$$

where $T_{0,in}$ is the total temperature of inlet flow, T_0 is the local total temperature, and T_c is the temperature of the coolant. The larger the θ is, the more dominant the coolant is. For both the cooled flat tip and the cooled squealer tip, we could clearly observe the distributions of θ on corresponding planes (plane M and plane N). These two planes are perpendicular to the camber line and cross over the center of the cooling holes. Note that the θ is relatively large when the coolant was injected from the cooling holes, the profiles of high θ regions vividly illustrate the position of coolant core. The coolant core locally blocks the upstream OTL flow and forces fluids to bypass the coolant core.

Figure 11 shows the overall OTL flow structures on blade tip surfaces for cooled flat and squealer cases. The streamlines of the coolant (cold) and the upstream fluid (hot) are in blue and red respectively. Compared to the flat tip, a wider diffusion range of coolant is found for the cooling hole in the same position for the squealer tip. As shown by the white dotted lines, a portion of upstream fluid goes to the bottom of the coolant and intensifies the heat exchange on the tip surface. But the other part flows to the middle of the two branches of the CRVPs. This part is lifted and it makes the heat transfer on the tip surface weakened. It causes the existence of the thermal stripes on the cooled tip surfaces in Figure 12. Similar to the uncooled squealer tip, the fluid flows to the groove and the vortices are formed as the fluid hits the suction side rim in the frontal part of the blade tip.

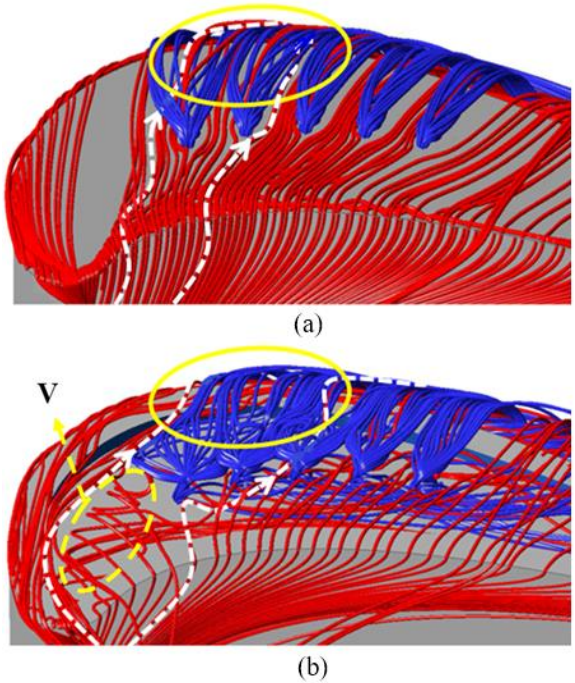

Fig. 11. Overall OTL flow streamlines for cooled flat and squealer cases

3.3 Heat Transfer Coefficients on Different Tip Geometries

Figure 12 compares the HTC on the tip surfaces of the four tip geometries, and the uncooled/cooled cases for flat and squealer tips are investigated. For all given cases, it is observed that an evident ridge of high HTC appears near the leading edge (marked A). The flow separates and then reattaches in region A. Similar to the region A, a striped high-HTC region is displayed along the edge near the pressure side. For the flat tips (including uncooled and cooled cases), the stripe of low HTC is found in region B. The profile of the striped low-HTC region in Figure 11(a) is in good accordance with the border of the normal shock wave in Figure 6.

It is found that the HTC distributions over the tip surfaces change greatly with the introduction of cooling injection. Compared to the uncooled flat tip in Figure 12(a), the area of the low-HTC stripe (region B) shrinks in Figure 12(c). And the striped high-HTC region is clearly visible in region C. Moreover, the value of HTC on the left side of the high-HTC stripe is larger than that on the right side. This is because the right branch of CRVP is more dominant than

the right branch on the tip surface. A similar analysis was carried through by Ma et al. [25].

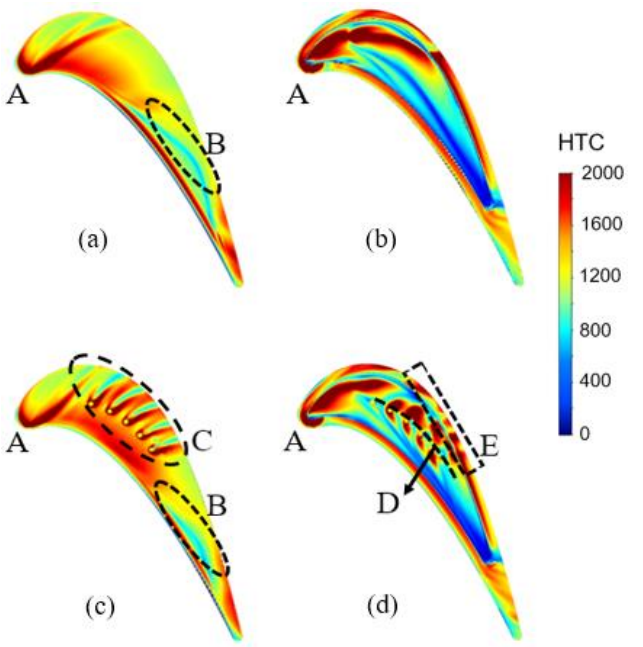

Fig. 12 Comparison of HTC on different tip geometries: (a) uncooled flat and squealer tips (b) cooled flat and squealer tips

For the cooled squealer tip in Figure 12(d), the high HTC regions can be observed on both sides of the camber line (marked D) except for the region around the first cooling hole. Note that a series of thermal stripes appear on the suction side rim (region E). These thermal stripes are mainly caused by the asymmetrical branches of the CRVP. It indicates that the cooling injection strongly influences the heat transfer over the tip surfaces.

4 Conclusions

The aerothermal characteristics of transonic OTL flow with the cooling injection for different blade tip geometries are numerically investigated. The simulations using SST k-ω model were observed to be in good agreement with the experimental result, especially for the low HTC regions on the cavity floor close to the pressure side and the high HTC regions near the leading edge.

For the flat tip, the reflected shock wave (the oblique shock wave) appears near the pressure side corner. There exists a high striped C_p region on the tip surfaces near the pressure side. And a normal shock wave is produced along the border of this region. It is found that the introduction of cooling injection reduces the range of the high striped C_p region. For the uncooled and cooled squealer tips, a larger flow separation zone makes the values of C_p on the surfaces of the suction side rim are bigger than those on the surfaces of the pressure side rim.

Driven by the big pressure difference, the OTL flow goes to the suction side and blends with the mainstream, forming the tip leakage vortex. And a considerable aerodynamic penalty was caused by such TLV for both the flat tip and squealer tip. However, the flat tip apparently shows a smaller stagnation pressure ratio near the casing and the tip surface than the squealer tip.

The coolant first hits the casing and then bifurcates into two branches, forming the counter-rotating vortex pair (CRVP). The coolant core, described by the nondimensional total temperature, locally blocks the upstream OTL flow and forces fluids to bypass the coolant core.

Another interesting observation is that the cooling injection greatly changes the heat transfer on the blade tip surfaces, especially for the area around the cooling holes and the downstream of such holes. And the branches of the CRVP cause the thermal stripes. It illustrates the cooling injection has a strong effect on heat transfer on the tip surfaces.

Acknowledgments

The authors gratefully acknowledge the support of China Scholarship Council, Chinese National Science Foundation (51506120, 51376127) and the Aeronautical Scientific Funding.

Nomenclature

C_p	=	pressure coefficient
CRVP	=	counter-rotating vortex pair
EXP	=	experiment
HPT	=	high pressure turbine
HTC	=	heat transfer coefficient
m''	=	mass flux
OTL	=	over-tip leakage
P	=	pressure
PS	=	pressure side
SS	=	suction side
TLV	=	tip leakage vortex
V	=	velocity, vortex
θ	=	nondimensional total temperature

Subscripts

c	=	coolant
exit	=	mainstream outlet
in	=	mainstream inlet
0	=	total

References

1. Ameri, A. A, Steinthorsson, E, Rigby, D. L (1999) Effects of Tip Clearance and Casing Recess on Heat Transfer and Stage Efficiency in Axial Turbines. ASME J Turbomach 121, pp. 683–693.
2. Ameri, A. A, Bunker, R. S (1999) Heat Transfer and Flow on the First Stage Blade Tip of a Power Generation Gas Turbine: Part II: Simulation Results. ASME J Turbomach 122, pp. 272–277.

3. Bunker, R. S, Bailey, J. C, Ameri, A. A (1999) Heat Transfer and Flow on the First Stage Blade Tip of a Power Generation Gas Turbine—Part I: Experimental Results. ASME Paper No. 99-GT-169.
4. Ameri, A. A (2001) Heat Transfer and Flow on the Blade Tip of a Gas Turbine Equipped with a Mean-Camber line Strip. ASME J Turbomach Vol. 123, No. 4, pp. 704–708.
5. Krishnababu, S. K, Newton, P. J, Dawes, W. N., Lock, G. D, Hodson, H. P, Hannis, J (2007) Aerothermal Investigations of Tip Leakage Flow in Axial Flow Turbines—Part I: Effect of Tip Geometry and Tip Clearance Gap. AMSE J Turbomach 131(1), pp. 727-738.
6. Krishnababu, S. K, Hodson, H. P, Dawes, W. N, Lock, G. D, Hannis, J, Whitney, C (2007) Aerothermal Investigations of Tip Leakage Flow in Axial Flow Turbines—Part II: Effects of Relative Casing Motion. ASME Paper No. GT2007-27957.
7. Newton, P, Lock, G. D, Krishnababu, S, Hodson, H, Dawes, W, Hannis, J, Whitney, C (2009) Aero-Thermal Investigation of Tip Leakage Flow in Axial Flow Turbines—Part III: Tip Cooling. ASME J Turbomach 131(1), p. 011008.
8. Yang H, Chen, H. C, Han J. C (2006) Turbine Rotor with Various Tip Configurations Flow and Heat Transfer Prediction. Journal of Thermophysics & Heat Transfer 20(1), pp. 80-91.
9. Yang, H, Chen, H. C, Han, J. C (2013) Flow and Heat Transfer Prediction on Turbine Rotor Blade with Various Tip Configurations. Journal of Thermo-physics & Heat Transfer 20(1), pp. 80-91.
10. Yang, H, Acharya, S, Ekkad, S. V, Prakash, C, Bunker, R (2002) Flow and Heat Transfer Predictions for a Flat-Tip Turbine Blade. ASME Paper GT-2002-30190.
11. Yang, H, Acharya, S, Ekkad, S. V, Prakash, C, Bunker, R (2002) Numerical Simulation of Flow and Heat Transfer Past a Turbine Blade with a Squealer-Tip. ASME Paper GT-2002-30193.
12. Azad, G. M. S, Han, J. C, Teng, S, Boyle, R (2000) Heat Transfer and Pressure Distributions on a Gas Turbine Blade Tip. ASME J Turbomach Vol. 122, No. 4, pp. 717–724.
13. Azad, G. M. S, Han, J. C, Boyle, R (2000) Heat Transfer and Pressure Distributions on the Squealer Tip of a Gas Turbine Blade. AMSE J Turbomach Vol. 122, No. 4, 2000, pp. 725–732.
14. Kwak, J. S, Han, J. C (2002) Heat Transfer Coefficient and Film Cooling Effectiveness on a Gas Turbine Blade Tip. ASME Paper No. 2002-GT-30194.
15. Kwak, J. S, Han, J. C, (2002) Heat Transfer Coefficient and Film Cooling Effectiveness on the Squealer Tip of a Gas Turbine Blade. ASME Paper No. 2002-GT-30555.
16. Kwak, J. S, Ahn, J, Han, J. C, Lee, C. P, Boyle, R, Gaugler, R (2003) Heat Transfer Coefficients on the Squealer Tip and Near Tip Regions of a Gas Turbine Blade with Single Squealer or Double Squealer) ASME Paper GT2003-38907.
17. Christophel, J. R, Thole, K. A (2005) Cooling the Tip of a Turbine Blade Using Pressure Side Holes—Part I: Adiabatic Effectiveness Measurements. ASME J Turbomach 127(2), pp. 270–277.
18. Christophel, J. R, Thole, K. A, Cunha, F. J (2005) Cooling the Tip of a Turbine Blade Using Pressure Side Holes—Part II: Heat Transfer Measurements. ASME J Turbomach 127(2), pp. 278–286.
19. Wheeler, A. P. S, Atkins, N. R, He, L (2011) Turbine Blade Tip Heat Transfer in Low Speed and High-Speed Flows. ASME J Turbomach Vol. 133, No. 4, pp. 041025-1–041025-9.
20. Zhang, Q, He, L, Wheeler, A, Ligrani, P, Cheong, B (2011) Over-tip Shock Wave Structure and Its Impact on Turbine Blade Tip Heat Transfer. ASME J Turbomach 133(4), p. 041001.
21. Couch, E, Christophel, J, Hohlfeld, E, Thole, K. A, Cunha, F. J (2005) Comparison of Measurements and Predictions for Blowing from a Turbine Blade Tip. AIAA J Propul Power 21(2), pp. 335–343.
22. Wheeler, A. P, Saleh, Z (2013) Effect of Cooling Injection on Transonic Tip Flows. AIAA J Propul Power 29(6), pp. 1374–1381.
23. Wheeler, A. P, Atkins, N. R, He, L (2011) Turbine Blade Tip Heat Transfer in Low Speed and High-Speed Flows. ASME J Turbomach 133(4), p. 041025.
24. Ma, H, Zhang, Q, He, L, Wang, Z, Wang, L (2016) Cooling Injection Effect on a Transonic Squealer Tip—Part I: Experimental Heat Transfer Results and CFD Validation. ASME Paper No. GT2016-57579.
25. Ma, H, Zhang, Q, He, L, Wang, Z, Wang, L (2016) Cooling Injection Effect on a Transonic Squealer Tip—Part II: Analysis of Aerothermal Interaction Physics. Journal of Engineering for Gas Turbines & Power 139(5), 052507.